2018-01-0213

An Experimental Study on the Knock Mitigation Effect of Coolant and Thermal Boundary Temperatures in Spark Ignited Engines

Author, co-author (Do NOT enter this information. It will be pulled from participant tab in MyTechZone)

Affiliation (Do NOT enter this information. It will be pulled from participant tab in MyTechZone)

Abstract

Increasing compression ratio is essential for developing future high-efficiency engines due to the intrinsic characteristics of spark-ignited engines. However, it also causes the unfavorable, abnormal knocking phenomena which is the auto-ignition in the unburned end-gas region. To cope with regulations, many researchers have been experimenting with various methods to suppress knock occurrence. In this paper, it is shown that cooling the combustion chamber using coolants, which is one of the most practical methods, has a strong effect on knock mitigation. Furthermore, the relationship between thermal boundary and coolant temperatures is shown.

In the beginning of this paper, knock metrics using an in-cylinder pressure sensor are explained for readers, even though entire research studies cannot be listed due to the innumerableness. The coolant passages for the cylinder head and the liner were separated to examine independent cooling strategies. In addition, piston surface temperature was changed through the oil supply to the piston oil gallery. To investigate the effects on the thermal boundary temperature under knocking conditions, temperatures were measured. Knock mitigation effects were quantified while the coolant temperatures were varied. Quantification in this study consists of two methods: The advancement of the crank angle ignition timing and the expansion of the borderline knock (detonation border line). The different impacts of cooling between PFI (port fuel injection) and GDI (gasoline direct injection) engines and the differences under various S/B (stroke-to-bore) ratios are also shown in this study.

After implementation, it was shown that decreasing the coolant temperature in the cylinder head has a greater effect than that of the liner. Furthermore, 4.2 CA and 5 CA of ignition timing advance and 10% and 6.8% of knock load limit expansion were achieved while the coolant temperature was decreased from 85℃ to 60℃ under 1500 rpm and 2000 rpm, respectively. GDI engine also showed knock mitigation effects by the coolant temperature decrease. Higher stroke-to-bore ratio led to expanded load limit due to increased knock suppression. However, there was no significant difference in the effect of coolant temperature decrease for various stroke-to-bore ratios.

Introduction

The most important development in spark-ignited engines is the increase of the compression ratio [1]. Because fuel economy regulation is becoming more stringent, industrial automotive makers and researchers are focused on increasing the efficiency of spark-ignited engines. Accordingly, the future development of higher compression ratio engines is now more active than ever before in the spark-ignited engine field. The compression ratio has a direct relationship with the efficiency in an ideal engine. Its theoretical characteristic is shown in Equation 1, where η is the efficiency, r_c is compression ratio, and γ is the polytropic coefficient.

$$\eta = 1 - \frac{1}{r_c^{\gamma-1}} \quad (1)$$

However, a higher compression ratio increases the occurrence of knock in-cylinder conditions because of the increased pressure and temperature in the unburned end-gas region.

Knock is auto-ignition in the unburned end-gas zone, as the flame propagation in the unburned end-gas zone is non-uniform and can be classified as three modes: deflagration, thermal explosion, or developing detonation [2, 3]. From the numerical study of Zeldovich et al. [4], König et al. [5] identified these modes and showed that auto-ignition of the hot-spot can lead to pressure spikes. Knock occurrence in spark-ignited engine must be avoided during operation because it can cause serious engine failure and damage [5, 6, 7]. An overview and the principle of knock is described by Wang et al. [8].

For knock mitigation or control during operation, car manufacturers previously utilized spark timing strategies. However, this method decreases efficiency and increases the exhaust temperature excessively, which may deteriorate the durability of downstream components. To solve this problem, exhaust cooling strategies such as over-fueling are frequently adapted. However, this also decreases the engine efficiency and increases CO and THC emissions [9].

In this chapter, more practical and fundamental methods of reducing knock occurrence are introduced. One is the enhancement of flame speed during the combustion process. Under the enhanced flame speed, the air-fuel mixture in the unburned end-gas area can be consumed before the in-cylinder condition reaches the auto-ignition point. Use of advanced ignition systems not only can increase the efficiency but also has an effect of knock suppression [10, 11, 12, 13, 14]. Introducing a high-tumble port design is also one of the most effective ways to produce fast combustion, which can produce higher turbulent intensity to increase flame speed [15, 16, 17, 18, 19].

Another method of improvement uses an EGR system. EGR is a very promising method for knock mitigation that reduces the in-cylinder temperature and reactivity of unburned end-gas. [19, 20] Companies put a great deal of effort into EGR systems because of its potential. Matsuo et al. [21] improved the manifold design to enhance the EGR distribution of each cylinder. Cooled EGR [10] and improved EGR cooling units [20] have recently been adapted to mass production engines.

The third method is the engine cooling strategy. Knock suppression with this method is achieved by decreasing the temperature of the air-fuel mixture in the cylinder by decreasing the wall temperatures. Lowering the coolant temperature reduces the amount of initial heat transfer to the mixture from the wall before the start of combustion and increases the heat transfer to the cylinder wall during the expansion stroke (heat loss). This eventually leads to the end-gas temperature decreasing, which can allow the unburned end-gas to be consumed before auto-ignition occurs. Improving the temperature distribution by structural changes using a water jacket [20, 21], enhancement of combustion chamber cooling such as the introduction of hollow valves [10], split cooling or dual-loop cooling system have been shown in recent studies [21].

Kobayashi et al. [22] introduced a dual circuit cooling system (referred as cooling segregation in authors' study) into a four-cylinder compression ratio of 9.0 1.3L engine and showed that the operating condition was affected more by the cylinder head coolant temperature than the block coolant temperature. The effect by lowering head coolant temperature was twice as much as that by lowering the cylinder block coolant temperature. Authors in the study explained that it is due to the lowering of cylinder head coolant temperature leading to a larger decrease of unburnt gas temperature during the combustion process caused by the larger wall temperature decrease.

Finlay et al. [23] demonstrated a precision cooling system to small automotive engines. Higher velocities of coolant showed higher heat flux through the combustion chamber wall, which resulted in up to 50℃ decrease of surface temperatures. Iwashita et al. [24] also investigated the effect of coolant flow. Their research showed higher velocities of the coolants can effectively reduce the wall temperatures which derived 2~4 CA additional advance of ignition timing.

Kubozuka et al. [25] developed an evaporative cooling system which has a superior cooling effect than a conventional liquid cooling system. Wall temperature could be controlled accurately by controlling the vapor pressure in the system. Using this system, 1 CA KLSA (knock limit spark advance) advance was achieved for every 10℃ drop in coolant temperature. (corresponding to 0.1 CA / ℃) Knocking characteristics for liquid cooling of 85℃ were similar to those for evaporative cooling at 90 to 100 ℃.

Russ [26] investigated the effect of various engine operating conditions on borderline knock including the coolant temperature. In this study, the effect of each operating parameter was quantified as a function of octane number. In terms of coolant, effects of coolant temperature variation were investigated and 10 K decrease of coolant temperature led to the corresponding effect of increasing one octane number of fuel. Independent cooling effect of the cylinder head and liner were also observed. It was found that volumetric efficiency was slightly more affected by the cylinder head temperature while the KLSA was more sensitive to the block temperature. It was shown the effects of head coolant and liner coolant were almost similar. The author explained the effect of engine block temperature on the unburned charge temperature by the end of compression is similar to the larger effect on the heat transfer of head to the charge during air induction. Furthermore, the effect of lowering the coolant temperature was more significant at the lower engine speed due to dilated time for heat transfer to the charge.

Fukuda et al. [27] employed a dual control direct cooling system with individual thermostats for cylinder head and block to 2.4 L DOHC engine. As a result, the temperature of cooling water in water jacket was lowered 23℃ average under similar conditions at WOT (wide open throttle), 6000 rpm. Knock limit was evaluated by using the system and showed an improvement of 6.3 CA advance compared to the baseline of single control cooling system at 6,000 rpm.

Dakahashi et al. [28], in their 3-D CFD simulation work, showed the potential of the liner temperature distribution affecting the auto-ignition in the cylinder. In their paper, they explained that the in-cylinder air mixture temperature is affected by the exhaust side of the cylinder liner rather than the intake side due to intake air flow motion at the beginning of the intake process. Therefore, to reduce the ring friction loss of the piston, they proposed strategic cooling that increases the liner temperature on the intake side and decreases the exhaust side temperature.

Imaoka et al. [29] investigated the effect of wall temperature on knocking combustion under high compression ratio conditions. Through extensive experimental and computational approaches, it has been shown that the heat transfer towards the intake air charge from the intake port is dominant in the temperature increase. Furthermore, a few independent coolant passages were designed for the test, and as a result, ignition timing could be advanced by decreasing the coolant temperature. Furthermore, the authors introduced the optical method and, through CFD work, found the squish in the chamber has an effect on knock mitigation due to its large heat transfer effect to the wall from the unburned gas.

Asif et al. [9] investigated the effect of coolant on KLSA using a multi-cylinder DISI engine with dual CVVT (continuous variable valve timing) system. They showed in their recent study that the temperature between the exhaust valve bridge decreases by only 1℃, while the coolant flow decreases by 20%. KLSA was not significantly affected by the reduction of the flow. Moreover, they observed KLSA was retarded from approximately 0.5 CA to 1 CA while the coolant temperature increased from 90℃ to 100℃. They explained this variation cannot be considered a significant change in the paper.

Cho et al. [30], the authors of this study, have observed the effect of coolant experimentally in a wider temperature range. With a steady-state experiment using a single-cylinder SI engine, it was shown that by decreasing the coolant temperature, knock can be mitigated during operation effectively. Using a segregated cooling system for the cylinder head and the liner, and maintaining MBT (maximum brake torque) timing at every operating condition, the expansion of the maximum operable load was achieved. While maintaining the same load, it was shown that approximately 0.2 CA of ignition timing advance was achieved for every 1℃ decrease of the coolant temperature. Furthermore, using the optical method and a PCB (printed circuit board) flame ionization gasket, location search of the knock occurrence spot was facilitated. As a result, under the operating conditions, the intake and exhaust side in the cylinder were found to be the main locations where auto-ignition occurs. It was also shown that coolant temperature variation does not have a significant influence on knock location.

This study verifies the influence of coolant temperature variation on each wall temperature of the combustion chamber. In addition, the knock suppression effect of reduced coolant temperature was quantified in two ways: ignition timing advance and maximum load expansion in certain operating conditions. The effects under different engine types are also investigated: PFI and GDI, and under various stroke-to-bore ratios: 1.0, 1.2, 1.47.

Knock Metrics: in-cylinder pressure sensor

There are various approaches for knock detection and analysis that highly depend on the tester. This was already described as a dilemma in the knock research field by Kalghatgi et al. [31] in a recent study. This chapter describes the metrics commonly used in knock research and testing field.

Knock detection method

In this study, the method with an in-cylinder pressure sensor was adapted. This is the most versatile [9] and direct method among the various methods to detect knocking behavior. However, this type of measurement highly depends on the mounting position of the in-cylinder pressure sensor [32, 33]. Therefore, the sensor was mounted flush and bias positioned to one side of the cylinder head. This has already been shown as the most proper way to observe the in-cylinder pressure oscillation in previous studies. There are other methods to detect knock as well: vibration signal, ion current signal and exhaust temperature, etc. [34].

Many researchers have normally used high-pass (band-pass) filters for signal processing. There are a few ways to filter the signal; usually, Butterworth or median filtering methods are adopted. The former has the advantage of its characteristic for noise reduction but generates a bias after filtering so that the knock onset is determined incorrectly [35]. Under the condition of weak knocking combustion, this would be worse. This will be further discussed later in this chapter. Accordingly, during the experiments in this study, the Butterworth band-pass filter was adapted, and the MAPO (maximum amplitude of pressure oscillation) TVE (threshold value exceed) method was used to detect knock occurrence [30]. In addition, for more sophisticated analysis for knock onset determination, to prevent the aforementioned bias after band-pass filtering, a 9-point (corresponding to 0.9 CA) median filter with Savitzky-Golay smooth-filtering was adapted. This will be shown later in this paper.

Draper [36] solved the wave equation and suggested the in-cylinder pressure oscillation mode that has been widely used in knock studies. Millo et al. [37] and Eng. et al. [38] also introduced the equation and showed the relationship between cylinder bore, sound speed and the radius of the cylinder bore. Gaeta et al. [39] showed advanced modeling of in-cylinder pressure oscillation under knocking condition including the damping mechanism, which can be from friction, heat transfer and expansion of the fluid. The solution and principle of the wave equation is well-written in many studies [36, 37, 38, 39, 40, 41]. The frequency of pressure oscillation can be expressed as Equation 2 [39].

$$f = \frac{\bar{a}}{2\pi} \cdot \sqrt{\left(\frac{\mu^*_{\lambda m}}{B/2}\right)^2 + \left(\frac{\pi g}{Z_0}\right)^2} \quad [Hz] \qquad (2)$$

$\mu^*_{\lambda m}$ is the m[th] root of the first derivative of Bessel's equation ($J'_\lambda(\mu^*_{\lambda m})=0$), where (m = 1, 2, ...) and (λ = 0, 1, ...). λ is the number of the circumferential mode, m is radial mode number and g is the axial mode number. $\bar{a}$ is the speed of sound, B is the radius of the cylinder bore and Z_0 is the height assuming the volume between the piston top and engine head at knock onset is cylindrical, $Z_0 = V_0 / \pi B^2$. The first six pressure oscillation modes of the used engine in this study is shown in Table 1 and Fig. 1 under a cylinder bore radius equal to 81 mm, assuming there is no axial mode, and the gas temperature is 2500 K and the polytropic coefficient is 1.4. (note: speed of sound $\bar{a}$ = square root of γRT) Therefore, from this background, a 4~28 kHz 5[th] order Butterworth band-pass filter was used for the test in this study.

Table 1. Theoretical frequency of pressure oscillation mode (B = 81 mm)

λ, m	1, 1	2, 1	0, 1	3, 1	4, 1	1, 2
$\mu^*_{\lambda m}$	1.841	3.054	3.832	4.201	5.318	5.332
Frequency [kHz]	7.26	12.03	15.11	16.55	20.95	21.0

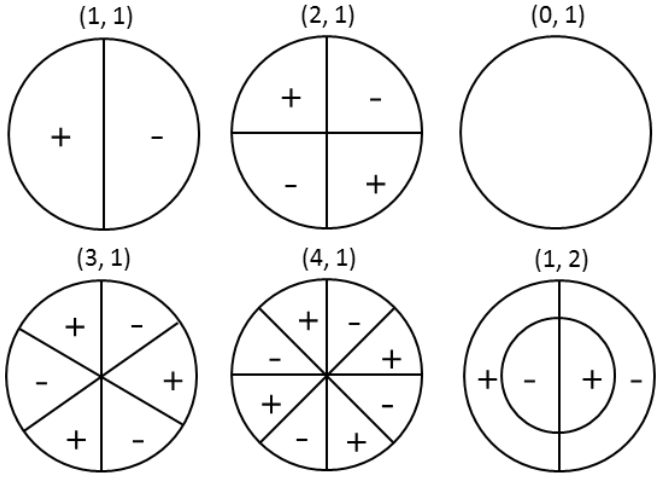

Figure 1. Schematic diagram of first six pressure oscillation modes (λ, m) by Draper [36]

Ando et al. [42] showed a good representativeness for the auto-ignition phase of the time interval between 50% to 10% of maximum heat release during the decay. Sjöberg et al. [43] defined 'strong end-gas auto-ignition' if the heat release of auto-ignition exceeds 75% of maximum heat release through the 1[st] law heat release calculation method. Very fast decay of heat release at the end of combustion was shown in the strong auto-ignition condition. From this observation, using ignition timing shaking method (maximum 5 CA), the auto-ignition combustion was clearly separated from the normal combustion under various fuel types. Kirsten et al. [44] proposed a new detection method and dimensionless indices for dual fuel combustion (Diesel/natural gas) using SOC (start of combustion) determination from heat release calculation, which showed good agreement.

However, knock detection with heat release calculation is not sensitive for especially weak knock detection and must rely on post-processing. This paper focuses on the thermal boundary condition,

which obviously has a strong relationship with auto-ignition and knock. Thus, a longer experiment time was essential to achieve the steady state condition, especially for the temperature. Longer experiment times can cause engine failure under knocking combustion, so every operating point was under weak knock condition, i.e., the method to detect the knock occurrence had to be sensitive enough to perform the correct statistics. Therefore, instead of the heat release calculation, in this study, the MAPO TVE method was used and it was determined as a knocking cycle if the maximum amplitude of the 4~28 kHz 5th order Butterworth band-pass filtered pressure signal exceeded the 0.5 bar of threshold. The 0.5 bar threshold of MAPO TVE is able to detect the knock at a lower intensity than a normal acoustic knock. (Brunt et al. [32] determined the acoustic knock for a knock intensity greater than two) This sensitive MAPO method still requires a high signal-to-noise ratio but can secure the engine durability during operation and results in more precise steady-state data. In most recent studies, McKenzie et al. [3] defined if the MAPO derived knock intensity exceeded 1 bar of threshold. Kalghatgi [31] used a 0.5 bar threshold of knock intensity, defined as twice the maximum amplitude of the pressure pulse.

Knock onset determination

There are two general ways to locate the knock onset during testing; one is the threshold value exceed method (TVE), and the other one is the signal energy ratio method (SER). The TVE method defines the knock onset as the crank angle when the amplitude of the high-pass filtered pressure signal exceeds the set threshold. Generally, this method has an error of 0.5 CA if the threshold is properly set [35]. Shahlari and Ghandhi [45] presented the SER method using SEPO (signal energy pressure oscillation), as shown in Equation 3, to compensate for the limitations of the TVE method. In their research, knock onset was defined as the timing when SER has the highest value, while a proper window size was suggested as 5 CA, and various filters were used for comparison.

$$\mathrm{SER} = \frac{SEPO_{fwd}{}^{2}}{SEPO_{bwd}{}^{0.5}} = \frac{(\int_{\theta_0}^{\theta_0+\Delta\theta} P_{filt}{}^{2} d\theta)^2}{(\int_{\theta_0-\Delta\theta}^{\theta_0} P_{filt}{}^{2} d\theta)^{0.5}} \qquad (3)$$

Researchers have found that the simple TVE method can possibly determine knock onset later than the actual onset [46]. To mitigate this defect, Lee et al. [47] compensated for a few crank angles earlier to reduce the difference. On the other hand, Kim [46] had found that the SER method can possibly determine knock onset earlier than the actual onset. Under these circumstances, Kim conducted an investigation on the TVE method to increase the accuracy of determining knock onset in the research. With the introduction of the standard deviation of median-smoothing high-pass filter, the knock onset was determined with more accuracy. In this paper, this method is referred to as the modified TVE method and was used to determine the knock onset with the pressure data from the experiment. For reference, in a recent study, Shahlari et al. [41] developed a new algorithm for determining the knock onset using an iteration method with very high accuracy.

The determination of knock onset is a critical aspect of knock analysis because a small error in knock onset can lead to a misunderstanding of combustion. For example, it is known that a 1 CA late determination of knock onset can result in an error of 5 bar for in-cylinder pressure and 5% of unburned mass fraction. Kim's [46] modified TVE method for knock onset determination seems to be outstanding when adapted to engine testing field without any modeling and simulation. It is simple, easy to calculate, and can be directly derived from the pressure data. In addition, it is well written in the reference because normal high-pass filters, such as Butterworth, result in a bias (observed as a dip in high-pass filtered signal) before the pressure oscillation spikes, and there is a possibility for incorrect detection. Thus, median-smoothing high-pass filtering was used.

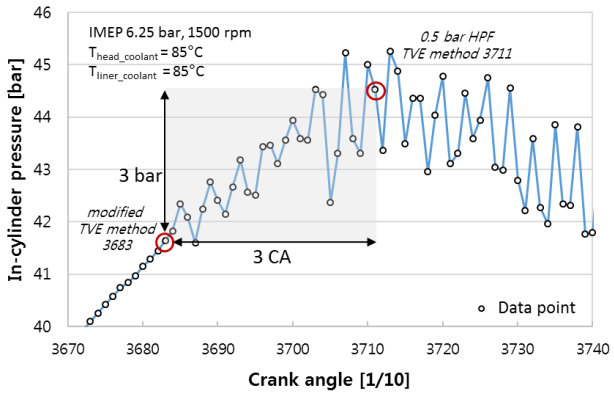

Figure 2. Comparison of modified [35] and normal TVE method for knock onset determination

In this study, based on Kim's modified TVE method, 9 data points were initially averaged (median filtering) from the raw in-cylinder pressure signal and trimmed using a Savitzky-Golay smoothing filter. (7 points, 2nd order) Then, a filtered signal was obtained by subtracting the trimmed signal from the original signal. The difference between the modified TVE method and normal MAPO TVE method is shown in Fig. 2. This is not extreme case but still shows a misdetection with approximately 3 CA and 3 bar discrepancy if a simple TVE method is used, considering that a 0.5 bar threshold value is already really small. Additionally, the greatest advantage of this method is its reliability under weak knock conditions.

Knock intensity calculation

For knock intensity calculations, the method also largely depends on the individual and operating conditions such as load, speed and shape of the engine. Borg et al. [48] showed a good comparison of various methods of knock intensity calculation. (MAPO, IMPO, ISPO, ringing intensity, etc.) It has been shown that time-domain calculations and frequency-domain calculations do not differ thanks to Parseval's identity [45].

Generally, researchers have investigated knock behavior using their own methods. It is generally accepted to use IMPO (integral of modulus of pressure oscillation), MAPO and ISPO methods for intensity calculations due to their simplicity and intuitiveness. (shown in Equation 4) Among the various methods, MAPO is the most commonly used. MAPO has the advantage of being able to be used in both software and hardware [48].

$$IMPO\ intensity = \frac{1}{N}\sum \int_{\theta_0}^{\theta_0+\Delta\theta} |P_{filt}| d\theta \qquad [bar \cdot deg]$$

$$MAPO\ intensity = max\left|P_{filt}\right|_{\theta_0}^{\theta_0+\Delta\theta} \quad [bar]$$

$$ISPO\ intensity = \int_{\theta_0}^{\theta_0+\Delta\theta} {P_{filt}}^2 d\theta \quad [bar^2 \cdot deg]$$

(4)

Brunt et al. [32] defined KI (knock intensity) as in Equation 5. A one-bar offset is applied so a knock pressure less than 1.0 bar does not contribute to the intensity calculation. This offset also has the advantage of zero being achievable when the ignition timing is retarded. (N_c = number or knocking cycle)

$$KI = \frac{20}{N_c}\sum(P_k - 1)$$

(5)

Amann et al. [49] used IMPO to calculate knock intensity in their study. Brecq et al. [50] established a new index, DKI (dimensionless knock indicator), which is a combination of IMPO and MAPO, as shown in Equation 6. (W = window size)

$$DKI = \frac{IMPO}{MAPO \times W}$$

(6)

Hudson et al. [51] introduced a new index called LKI (logarithmic knock intensity) using the energy concept as shown in Equation 7 (where C is a constant determined by trials). Then, a 6~25 kHZ band-pass filtered data was used for the average energy (which is ISPO) calculation. This was verified in the time and frequency domains. Additionally, it was shown that an analysis for knock intensity needs more than 1,000 units of cycle data.

$$LKI = ln(C \times \frac{1}{N}\sum_{n=0}^{N-1} x^2(n))$$

(7)

In very recent studies, Sjöberg et al. [43] calculated knock intensity using a 4~28 kHz frequency range of the signal to quantify the auto-ignition level. This filter range can include multiple modes of the acoustic waves. In the study, an average of 500 cycles was used. Bradley et al. [52] and Kalghatgi et al. [31] established knock intensity as twice the maximum amplitude of the pressure pulse. McKenzie et al. [3] used MAPO-calculated knock intensity. Mutzke et al. [53] validated MAPO, IMPO and LKI with measured heat flux. Shahlari et al. [41] developed a new method for determining knock intensity that can eliminate the potential bias from the transducer shock period, which is derived from a new method for knock onset determination. This seems to be the most progressive method for intensity calculation to date. However, this also requires post-processing after the experiment.

Knock incidence for engine test

Knock phenomena accompany cyclic variations and exhibit stochastic behavior [54]. For example, even if the same ignition timing is maintained, due to the variation of in-cylinder conditions, there is a considerable cyclic change on the occurrence timing (knock onset), frequency and intensity. For that reason, sometimes results of knock research are frequently shown with PDF (power density function) or other probabilistic terms, and it is important to decide how to measure and analyze the knocking phenomena precisely. In this study, to achieve precise steady-state conditions, the engine was operated in the long term under weak knock conditions. This also facilitated the calculation of knock intensity using 1,000 consecutive cycles. This is proposed by previous studies for less error considering the stochastic behavior of knock [32, 51]. For example, Brunt et al. [32] showed that approximately 50% of error was possibly made if 300 cycle data were used for the intensity calculation under weak knock conditions.

Because the occurrence and intensity of knocking phenomena is highly stochastic, to quantify the level of knock occurrence under a certain steady state condition, a representative index value is needed such as mean knock intensity. Furthermore, simpler logic leads to reduction of time and cost for installing system for tester. Therefore, in this study, MAPO knock incidence method (shown in Equation 8) was proposed and its validity was verified. This method can be easily adapted to any engine test facility with simple electronic circuit or computational code. The correlation was verified with a simple and fast ISPO (shown in Equation 8) method.

$$MAPO\ Incidence = \frac{N_{knock}}{N_{total}} \times 100 \quad [\%]$$

(8)

Knock intensity calculation under weak knock condition has a large error due to its stochastic characteristics (not enough samples) if knocking cycles are the only calculated measurement. Thus, For ISPO knock intensity calculation, 1,000 cycle overall value of the entire operating cycles was calculated. A 40 CA calculation window ($\Delta\theta$) was chosen, resulting in good performance. As previously mentioned, for validity of ISPO method, a correlation between ISPO method and other methods are thoroughly investigated and organized by Borg et al. [48], which showed larger than 0.9 of correlation coefficient with other indices under various conditions.

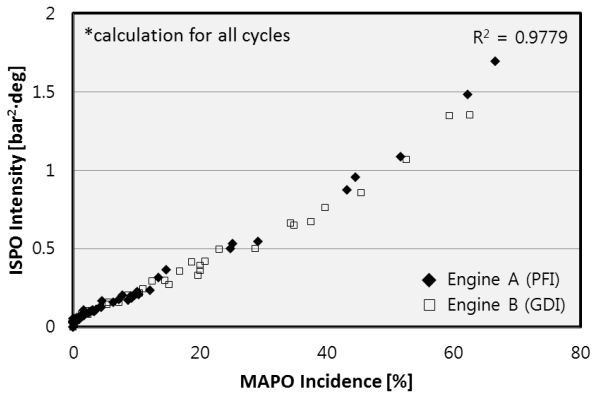

Figure 3. Correlation between knock intensity and knock incidence

The correlation between MAPO knock incidence and all-cycle ISPO knock intensity is shown in top graph of Fig. 3. It has a substantial correlation (R^2 = 0.98) with the conventionally calculated ISPO

knock intensity value. Besides, it is shown that two different engines used in this study all show good correlations.

From the validation result, it was concluded that the MAPO knock incidence method can represent the knocking behavior of engine operation. In this study, most of the test condition was maintained at 5% of knock incidence. (10% for oil-gallery cooling implementation)

Experimental Setup and Conditions

Engine setup and measurement

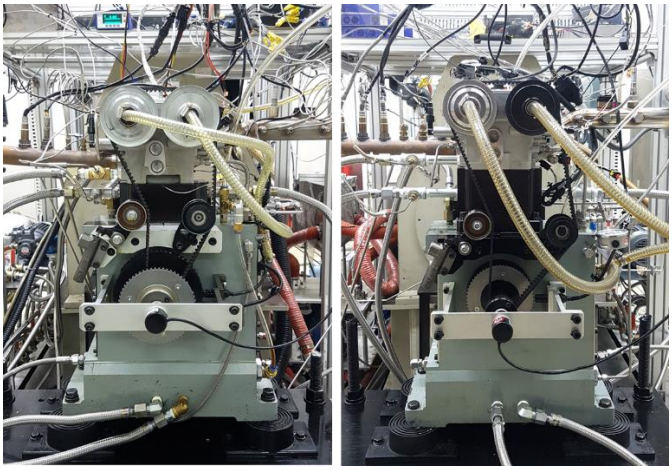

Figure 4. Single cylinder engines. A: MPI engine (left), B: GDI engine (right) for various S/B ratios

Two types of 0.5 L single cylinder engines were used, and both engines were equipped with CVVT systems. Four engines were used in total: A, B-1, B-2, B-3. Engine A is a natural aspirated dual PFI engine with two port fuel injectors. Engine B is a LIVC (late intake valve closing) Atkinson cycled GDI engine, which has 280 degrees of intake valve duration and 240 degrees of exhaust valve duration, respectively. Engine B was designed for various S/B (stroke-to-bore) ratios. In this study, three different S/B ratios were examined under the same compression ratio of 12 to eliminate other sources of error. Both engines are shown in Fig. 4, and the detailed engine specifications are shown in Table. 2.

It is important to mount the in-cylinder pressure sensor properly to obtain a fine signal to analyze knock. The pressure sensor was mounted flush in the cylinder head to minimize the cavity resonance and obtain higher sensitivity for pressure oscillation measurement [32, 36]. A Kistler 6056A piezoelectric in-cylinder pressure sensor was used instead of a spark-plug integrated sensor and was positioned biased from the centerline of the cylinder to measure pressure oscillation as much as possible. The proper location of the in-cylinder pressure sensor for knock detection has been well researched in previous studies [32, 33].

The schematic diagram of the engine testing system is shown in Fig. 5. AVL Indi Micro IFEM was used to amplify the in-cylinder pressure signal, and intake manifold pressure was measured with a Kistler 4045A2 absolute pressure sensor and the signal was amplified by a Kistler 4603 piezo-resistive amplifier. Pressure pegging was conducted at BDC ± 2CA during the intake process before combustion. To reduce the error caused by the TDC calibration using an in-cylinder pressure sensor, TDC was calibrated at mid-speed range (2500 rpm) and introduced 0.3 CA of heat loss angle. This method can still result in errors, especially while the engine is changed from B-1 to B-3; however, the compression ratio was held constant (± 0.05), so it was assumed that the loss angle is the same in this study.

Table 2. Detailed engine specifications.

Engine		Engine A	Engine B		
			B - 1	B - 2	B - 3
Type of engine		Single-cylinder N/A dual CVVT	Single-cylinder Atkinson-cycled dual CVVT		
Displacement [cc]		499.8	499.6	499.8	498
Stroke [mm]		97	86	97	111
Bore [mm]		81	86	81	75.6
Stroke-to-Bore ratio		1.2	1.0	1.2	1.47
Compression ratio		12			
Injection system		Dual PFI (3.5 bar)	Multi-hole GDI (100 bar)		
Injection timing		bTDC 540°	bTDC 330°		
Valve Timing (0.1 mm)	EVO	bBDC 68°	bBDC 59°		
	EVC	aTDC 1°	aTDC 1°		
	IVO	aTDC 10°	bTDC 34.5°		
	IVC	aBDC 67°	aBDC 65.5°		
Number of valves		4	4		
Max valve lift		10 mm	9.5 mm		

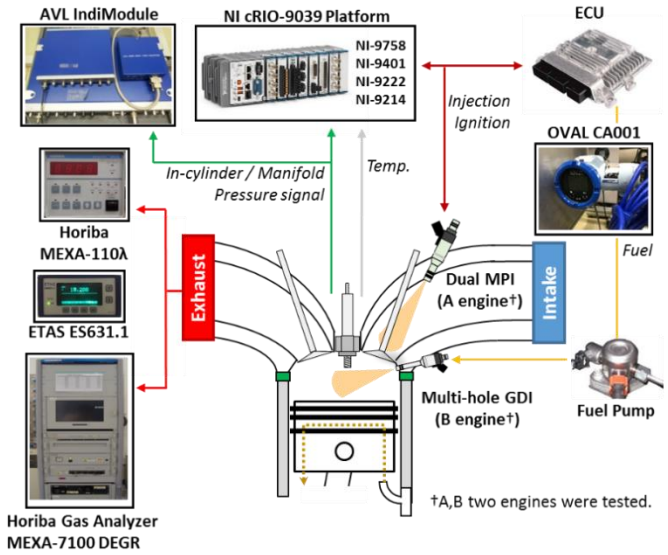

Figure 5. Schematic diagram of the engine experiment

To analyze the knock phenomena precisely, a high sampling rate is required because of the measurement of the pressure oscillations. Therefore, an encoder with 0.1 CA resolution was used. This was already shown to be sufficient for proper measurement [55, 56]. Combustion data was logged with an AVL Indi-module device. As

mentioned in the previous section, for the calculations related to knock measurement, 1,000 consecutive cycle data are used because fewer than 1,000 cycle data were not appropriate for analysis due to the stochastic behavior of knock. For combustion metrics, such as calculation for IMEP (indicated mean effective pressure) and MFB50 (mass fraction burned 50%), 300 cycle data are used. This number of cycles is necessary for proper combustion analysis [32, 56]. To obtain accurate fuel flow measurements using OVAL CA001, frequency output of the pulse signal was used instead of analog output signal to minimize signal loss and three-minute ensemble averaged values were used for calculation. This can achieve higher signal-to-noise ratios (S/N ~ $(n)^{0.5}$, n: number of repetitions [57]). Consequently, the error, except for the steady-state error of fuel flow measurement, was less than 0.3% in all operating conditions.

Horiba MEXA-110λ and ETAS ES631.1 were used to monitor the air-fuel ratio during operation to maintain a stoichiometric condition. A Horiba MEXA-7100DEGR exhaust gas analyzer was used to measure emissions. To control and further acquire data for knock and temperatures, an ECU combined with National Instrument cRIO-9039 platform and a few modules was used with developed code using LabVIEW software. (Modules: NI-9758: injection and throttle control, NI-9401: sync, ignition control, NI-9222: pressure signals, NI-9214: temperature)

Test conditions

Since four different types of engines were tested in this study, conditional similarity is necessary. Thus, to minimize the effect of different engine types (A: normal cam, B: LIVC cam), engine B was operated under the intake cam timing, which makes the motoring pressure the same as in engine A, while the exhaust cam timing was fully advanced. This resulted in the effective compression ratio being the same in this study.

The fuel properties are shown in Table 3, and test conditions are shown in Table 4. Knock incidence was mostly maintained at 5% for all operating conditions in this study (10% for oil-gallery cooling implementation), which means 5% of total operating cycles were classified as knocking conditions. By measuring 1,000 cycle data, weak knock condition with steady state condition is well achieved. The metrics for knock measurement and determination in this study are well interpreted in the previous chapter.

Table 3. Fuel properties

Conventional gasoline	Value	Test Method
H/C ratio	2.064	ASTM D 5291
Density [kg/m^3] @ 15℃	724.5	ASTM D 1298
Research Octane Number	91.5	ASTM D 2699
LHV [MJ/kg]	42.825	ASTM D 240-14
Oxygen [% in mass]	1.53	ASTM D 4815
Methanol [% in mass]	< 0.05	ASTM D 4815

In practice, the cooling water temperature has been tested from 85℃ to 40℃, but excessive cooling, such as 40℃, of coolant temperature may decrease the brake thermal efficiency since it requires more accessory work. Therefore, this study mainly focused on the conditions until down to the 60℃ condition. Cooling passages for the cylinder liner and the head were separated and controlled independently. Moreover, to maintain a uniform thermal boundary temperature, coolant flow was maximized. Consequently, the coolant temperature discrepancy between the inlet and outlet was less than 1℃ for all operating conditions. The piston surface temperature was controlled by the oil flow injected from the oil-jet. Authors have tried controlling the oil temperature to cool more excessively (20℃) but the oil was affected by the heat transfer and applied heat again in the oil passage before the injection. Tests were performed for 1500 rpm and 2000 rpm, and other information is shown in Table. 4.

Table 4. Test conditions

Engine speed [rpm]		1500, 2000
Air-fuel ratio		Stoichiometric (λ = 1)
Coolant Temperature [℃]	Head [℃]	60 ~ 85
	Liner [℃]	60 ~ 85
	Piston oil-jet	On / Off
Oil temperature [℃]		75 ± 1
Ambient temperature [℃]		30 ± 0.5
Fuel inlet temperature [℃]		35 ± 2

Experimental results and discussion

In this chapter, three main categories are discussed. First, the effect of independent cooling on each thermal boundary temperature is discussed. Second, the effect of cooling on knock mitigation is investigated using two methods: advance of ignition timing under the same load and expansion of maximum load. Third, the effect in different engines are shown: PFI and GDI and the impacts on different S/B ratio engines.

Thermal effect of cooling segregation

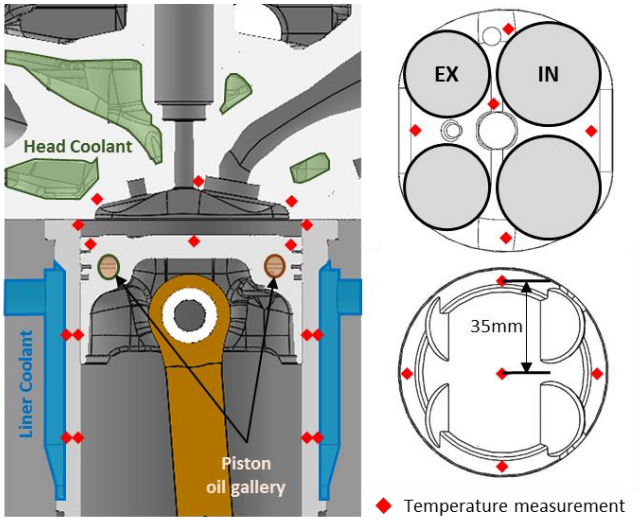

Figure 6. Shape of segregated cooling passage and temperature measurement positions.

The temperature measurement points for the thermal boundaries are shown in Fig. 6. All the points are located exactly 1 mm outside of the combustion chamber. Twenty-two total points were measured with K-type thermocouples: twelve points in the liner around the cylinder bore, inner wall and outer surfaces, five points beneath the top surface of the piston (including the center), five points in the cylinder head (including next to the spark-plug). Engine A was used, and an optimized linkage system was used to measure the piston temperature. [30] In this paper, the average temperature values are used.

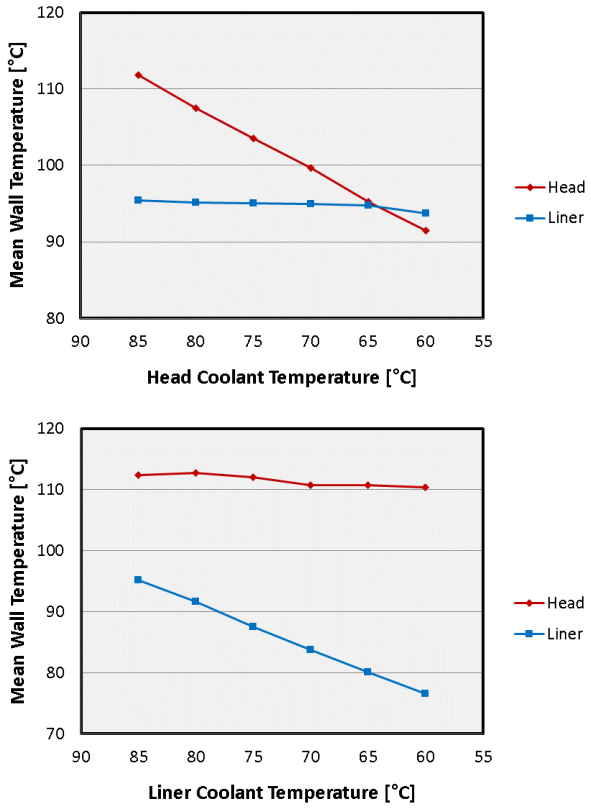

Figure 7. Head and liner wall temperatures: (a) Head cooling, (b) Liner cooling at IMEP 6 bar, 1500 rpm.

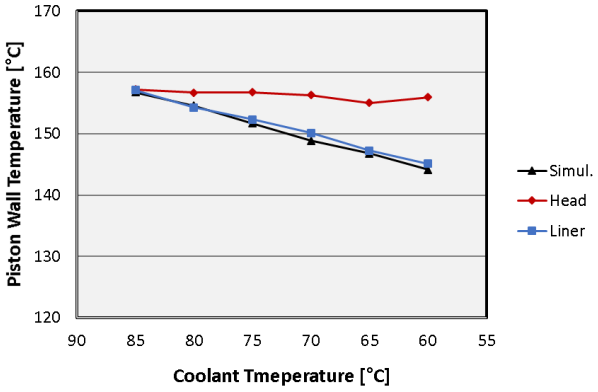

Figure 8. Piston wall temperature of piston at IMEP 7 bar, 1500 rpm.

The wall temperature variation of the head and liner are shown in Fig. 7. Experimental condition was 1500 rpm, IMEP 6 bar. While one of the two coolant temperatures were controlled, the other temperature was maintained at 85℃. From left to right on the X-axis, the coolant temperature decreases from 85℃ to 60℃. For example, in the top graph of Fig. 7, the red line with circular dots indicates the average head wall temperature against the head coolant temperature, while the liner coolant temperature remained constant at 85℃. It is clearly shown that cooling segregation was facilitated by independent cooling strategy. The mean wall temperature of the liner doesn't change significantly, while the head coolant temperature decreases. Likewise, the mean wall temperature of the head doesn't change a lot while cooling the liner. It can be concluded that the wall temperature of each component is dominantly determined by the coolant temperature. To avoid confusion, the result only shows the 1500 rpm case, but the tendency is the same for the 2000 rpm case as well.

In Fig. 8, the averaged piston temperature at 1500 rpm and IMEP 7 bar is shown (note that the wall temperatures in this study is 1 mm outside from the actual surface). Simul. indicates simultaneous decrease of the coolant temperatures for the head and the liner. Likewise, the red line with red circles indicates the piston wall temperature variation while only cooling the head coolant to 60℃. It is obviously shown that piston wall temperature is mostly affected by the liner because it shows almost no change when only the head coolant temperature decreases. This is thought to be due to a large amount of conduction through the piston rings. It is also shown that piston wall temperature variation is smaller than that of the liner when the liner coolant temperature decreases.

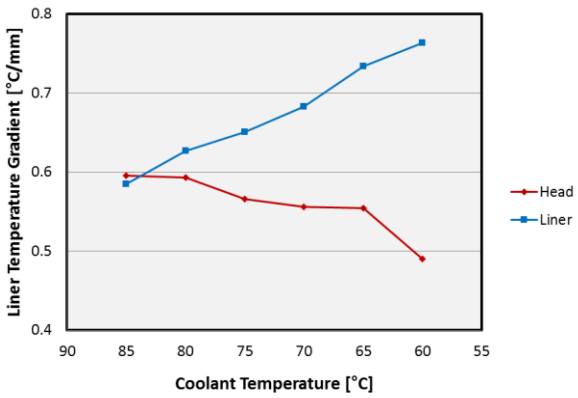

Figure 9. Temperature gradient of the liner wall at IMEP 6 bar, 1500rpm.

In Fig. 9, the temperature gradient (ΔT/mm) of the liner between 1mm outside from combustion chamber (5 mm inside the liner) and the outer surface is shown. Because temperature can be largely affected by the conduction by the cylinder head through the gasket, the location of 40.5 mm vertically lower from the liner top was selected. Intake and exhaust side both were measured and averaged. The gradient indicates the heat loss amount by the cylinder liner indirectly. Heat loss towards the liner is significantly affected by the head coolant temperature as indicated by the red line in the figure. As the head coolant temperature decreases, the heat loss toward the liner decreases as expected. Moreover, it increases considerably as the liner coolant temperature decreases. (The blue line in Fig. 9)

When the liner coolant temperature decreases, the amount of heat loss increases more quickly than that of heat loss decrease when cooling the head (the absolute slope of blue line is bigger than the

absolute slope of red line). Although the head cooling strategy is known to have a larger effect on knock mitigation than the liner cooling strategy (will be discussed later), since the piston temperature is not significantly affected by the cylinder head coolant temperature change, the liner also has great potential to reduce the gas temperature of the combustion chamber especially at the end-gas region or relatively low piston position such as intake process.

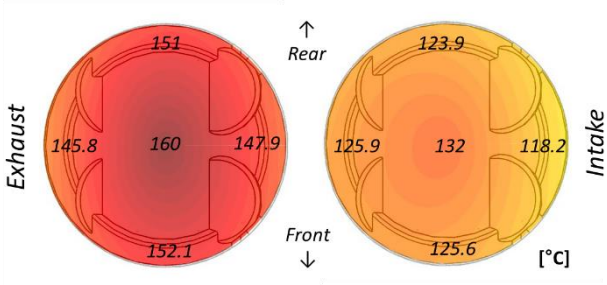

Figure 10. The temperature distribution of the piston at IMEP 7 bar, 1500 rpm: (a) oil-jet on, (b) oil-jet off

Figure 10 shows the measured temperature distribution of the piston with no-oil injection (left) and oil injection (right) at 1500 rpm, IMEP 7 bar. It is clear that the distribution changes when oil-gallery cooling is applied. The hot area moves to the exhaust side along with the decrease of the entire piston temperature. The temperature difference between the intake side and exhaust side increased when oil injection to the gallery is used. In these conditions, the difference of averaged coolant temperature between inlet and outlet was less than a 1℃ difference as well. Hwang et al. [10] showed a 17℃ decrease in the piston crown temperature using computational methods; however, the cooling effect was more substantial in this experimental study.

Advance of ignition timing

It is well known that ignition timing can be advanced if knock is suppressed. Figure 11 shows ignition timing advance under the same load condition, while knock mitigation was achieved through the coolant temperature being varied from 60℃ to 85℃. If the coolant temperature is high, for the same level of knock incidence, ignition timing had to be retarded which increases the amount of air-fuel mixture required to maintain the same load. The test procedure in this chapter is as follows.

(1) Determine the load limit at 60℃ coolant temperature

MBT was required. If the load is not enough at MBT timing, auto-ignition does not occur. Therefore, the load limit was first found for each coolant temperature condition. For example, under 1500 rpm, the IMEP for simultaneous cooling was 6.89 bar, 6.69 bar for head cooling and 6.54 bar for liner cooling.

(2) Determine the ignition timing at the test condition (varying the coolant temperature)

Maintaining the load and 5% knock incidence, appropriate ignition timing was determined for each condition. As the coolant temperature was increased, further retard of the ignition was necessary, and the air was induced more as ignition timing was retarded. All conditions maintained stoichiometric during the operation.

Approximately 0.2 CA of ignition timing advance was achieved for every 1℃ decrease of coolant temperature in the 1500 rpm simultaneous cooling case, as shown in Fig. 11. In all, 0.12 CA was achieved when the head coolant temperature was decreased 1℃, and 0.11 CA was achieved for liner cooling. The same implementation was conducted at 2000 rpm and resulted in 0.26 CA, 0.21 CA, 0.18 CA ignition advance for simultaneous, head, and liner cooling, respectively.

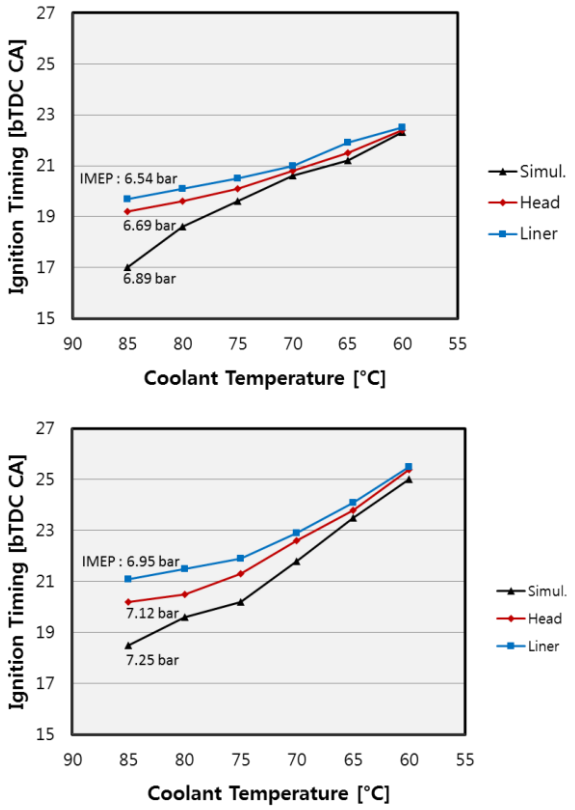

Figure 11. Ignition timing advance: (a) 1500 rpm, (b) 2000 rpm

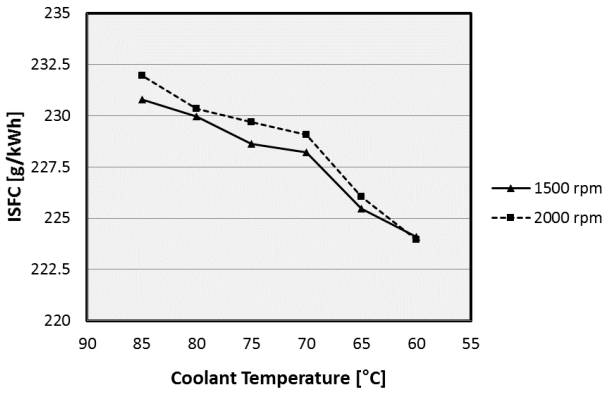

Figure 12. Indicated specific fuel consumption of simultaneous cooling.

The efficiency increase of the simultaneous cooling case is shown in Fig. 12 in terms of ISFC. A total of 2.89% and 3.45% of ISFC decrease was achieved at 1500 rpm and 2000 rpm, respectively, while the coolant temperature decreased simultaneously to 60℃. The trend

of ignition timing advance was identical until the temperature condition of 40℃ (excessive cooling). However, during engine operation, PM emission was excessive due to the poor fuel evaporation and seemed undesirable. Therefore, it was excluded in this paper.

Simultaneous cooling resulted in the largest absolute slope in the graphs and can be thought of as having the largest knock mitigation effect. Decreasing the head coolant temperature resulted in a larger slope in the figure than decreasing the liner coolant temperature. The potential of the liner part was already discussed in the previous chapter. However, even though the potential of the liner cooling was found through observing the heat loss, the cylinder head has a greater influence on knock behavior compared to the liner. This implies the temperature of the cylinder head contributes more to determining the end-gas temperature when auto-ignition occurs compared to heat loss towards the wall. This trend is also shown in the load expansion cases later in this paper. Heat transferred towards the intake air from the intake port, valves, etc. is thought to have a large influence and was investigated using CFD simulation by Imaoka et al. [29] in a recent study.

Expansion of load limit

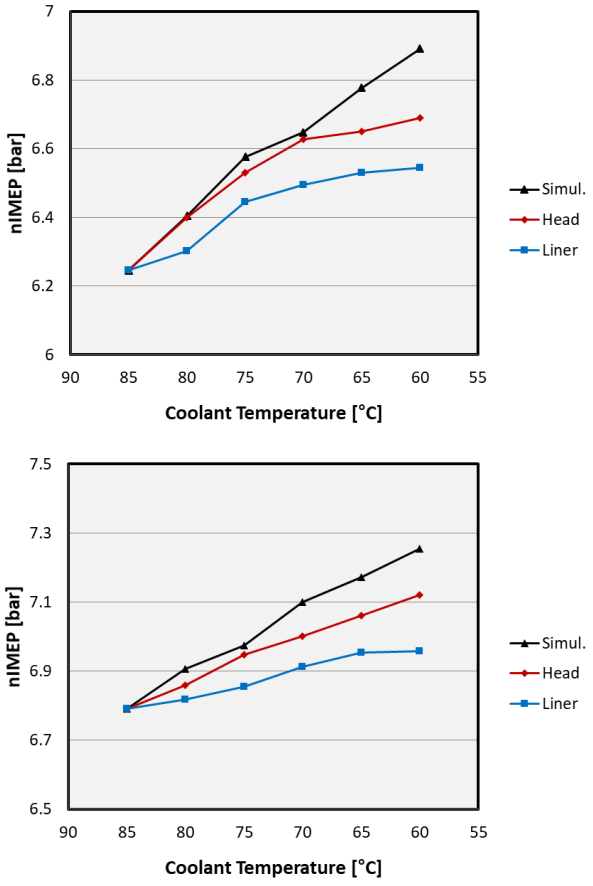

Figure 13. Load limit expansion, engine A (PFI): 1500 rpm, (b) 2000 rpm

In this study, load limit expansion was attempted while the coolant temperatures were decreased. The test was conducted at 1500 rpm and 2000 rpm, and load limit expansion was possible as further knock mitigation was achieved. The test method was as follows.

(1) Increase the load until 5% knock incidence was obtained at a coolant temperature of 85℃. MBT was maintained in all operating points. (aTDC 8 CA) All conditions maintained stoichiometric during the operation.

(2) Further increase the load at test condition (varying coolant temperature) maintaining 5% of knock incidence.

Figure 13 shows the results of load limit expansion while the coolant temperatures were controlled under 1500 rpm and 2000 rpm. As expected, the simultaneous cooling case showed the largest effect. The black line with triangles is the simultaneous cooling case, the red line with circles is the case where only the cylinder head was cooled while the liner coolant temperature was maintained at 85℃. The blue line indicates the opposite case. A significant difference in the knock mitigation effect between the head and the liner is shown in Fig. 13. Decreasing coolant temperature does not lead to deterioration of the efficiency. The efficiency increased from 36.79% to 37.03% during simultaneous cooling from 85℃ to 60℃ at 1500 rpm (there was no significant change at 2000 rpm). As a result, 10.3% and 6.8% of the load limit expansion was achieved in terms of IMEP at 1500 rpm and 2000 rpm, respectively, during simultaneous cooling. A 7.1% and 4.8% increase for head coolant cooling and a 4.8% and 2.5% increase for liner coolant cooling were achieved at the speed conditions. At 1500 rpm, 0.29% knock limit improvement was achieved for every unit temperature decrease of the head coolant. 0.19% was shown for liner cooling, 0.41% was shown for simultaneous cooling case. Likewise, at 2000 rpm, the load increase effect of 0.27% for simultaneous cooling, 0.19% for head cooling, 0.1% for liner cooling were achieved while decreasing 1℃ of the coolant. The ratio of effects on knock mitigation of each component can be generally said as follows.

Simultaneous : head : liner = 2.5 : 1.7 : 1.

The knock mitigation effect was quantified in two ways in this paper: ignition timing advance and load limit expansion. Ignition timing advance is more practical because it increases efficiency directly. However, every engine has different knock characteristics. For example, different maximum load, different combustion phasing for MBT, etc. make comparing different engines difficult when using the quantification of ignition timing advance method. Therefore, in the later part of this study, the load limit expansion method was used to compare various engine types.

Different engine type (PFI and GDI)

In previous section, only engine A (PFI) was used. In this chapter, the different behavior of engine B-2, which is GDI type with the same bore and stroke, is shown. As it is mentioned in the test condition chapter, the B-2 engine was operated under intake cam timing, which makes the motoring pressure equal to engine A, while the exhaust cam timing was fully advanced.

The overall load limit is higher than in engine A (PFI) under the same knock incidence (6.25 → 7.34 bar at 1500 rpm, 6.79 → 7.6 bar at 2000 rpm), as shown in Fig. 14. It is well known that GDI engine has higher resistance on knock due to the charge cooling effect of direct injected fuel. Unlike the PFI engine case, the effect of wall temperature decrease was increased in higher engine speed condition. While decreasing the coolant temperature simultaneously until 60℃, 9.6% and 11.1% of load limit expansion was achieved in 1500 and 2000 rpm, respectively. It was also shown that the decrease of head coolant temperature had larger effect on the knock mitigation than

that of liner coolant temperature. At 1500 rpm, 0.23% knock limit improvement for every unit temperature decrease of head coolant temperature. 0.098% was shown for liner cooling corresponding to a half effect of the head cooling, 0.42% was shown for simultaneous cooling case. Likewise, at 2000 rpm, 0.45% for simultaneous cooling, 0.22% for head cooling, 0.15% for liner cooling load increases were achieved while decreasing 1℃ temperature of the coolant. The ratio of mitigation effect in Engine B can be generally assumed as follows.

Simultaneous : head : liner = 3.5 : 1.9 : 1.

The effect by lowering head coolant temperature was approximately twice as much as that by lowering the liner coolant temperature in both PFI and GDI engines. This was also verified by Kobayashi [22] et al. However, the effect of simultaneous cooling of GDI engine is larger than that of PFI engine case. It is not clear why simultaneous cooling case shows additional effect in GDI engines. This still needs a further investigation.

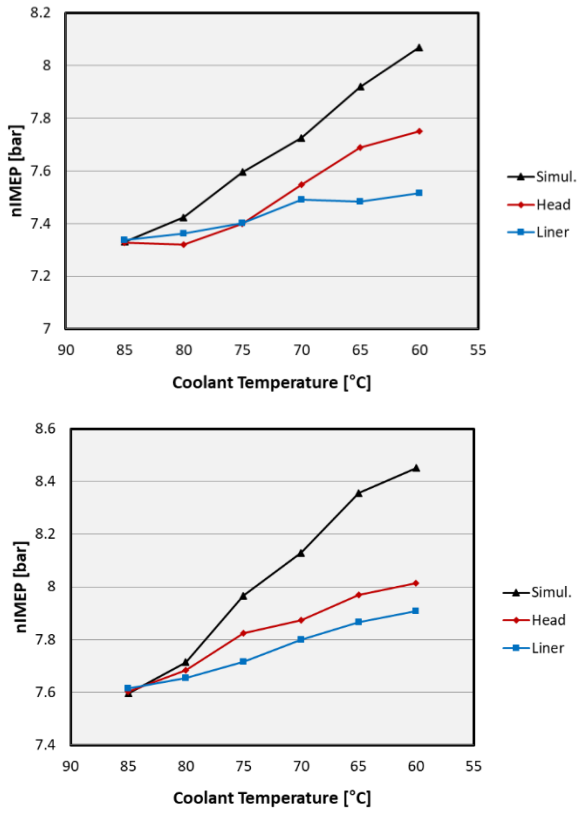

Figure 14. Load limit expansion, engine B-2 (GDI): (a) 1500 rpm, (b) 2000 rpm

Different stroke-to-bore ratio

Using engine B-1, 2, 3 described in Table 1, load limit expansion was implemented for various stroke-to-bore ratios. The compression ratio was the same (12 ± 0.05) as the aforementioned design concept. The shape of the heads and pistons are shown in Fig. 15.

Figure 16 shows the results of simultaneous cooling at 1500 rpm and 2000 rpm. Different S/B ratios also show similar effects. All the engine heads were designed to be a 1.3 tumble ratio (tested in tumble bench); however, mainly because of the mean piston speed, the turbulent energy of in-cylinder flow is thought to increase and leads to a lower burn angle as shown in fig. 17. Consequently, at higher S/B ratios, auto-ignition is effectively suppressed so the possibility of unburned end-gas being consumed before auto-ignition occurs increases. This is shown as higher load values in the figure for all coolant temperature conditions.

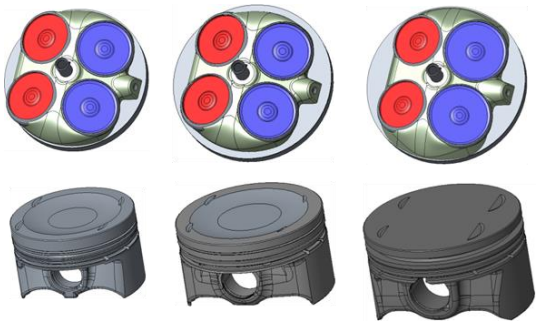

Figure 15. Shape of the cylinder heads and pistons for different S/B = 1.47, 1.2, 1.0 with CR = 12.

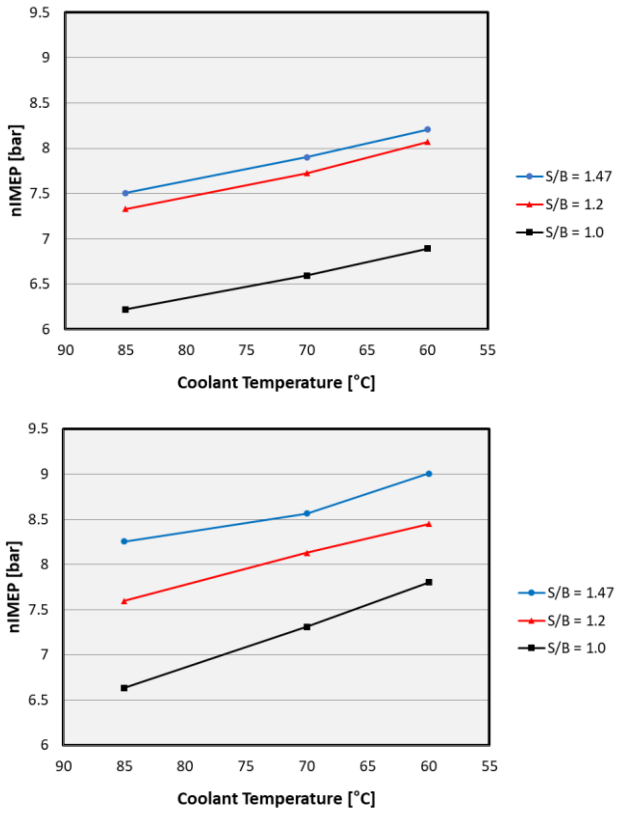

Figure 16. Load limit expansion for various S/B ratios (a) 1500 rpm, (b) 2000 rpm

However, at 1500 rpm, in the S/B = 1.47 case, the load limit was not significantly expanded compared to S/B = 1.2 case. At 2000 rpm, as S/B increases, burn duration was clearly decreased due to the increased mean piston speed. However, there was no significant difference in burn duration at 2000 rpm. Nevertheless, the load limit was expanded for larger S/B ratios. It can be concluded that not only flame speed is a dominant factor in knocking tendency, but the heat transfer between walls and air-fuel mixtures also have a large effect.

This still needs a further investigation. At the simultaneous 85℃ condition, averaged knock onset timings were 12.2°, 11.4° and 12° aTDC for S/B=1.0, 1.2 and 1.47 at 1500 rpm respectively. Likewise, 11.3°, 11.5° aTDC CA and 10.6° aTDC CA for S/B=1.0, 1.2 and 1.47 at 2000 rpm were shown. No significant difference of knock onset timing was observed under the three S/B ratios.

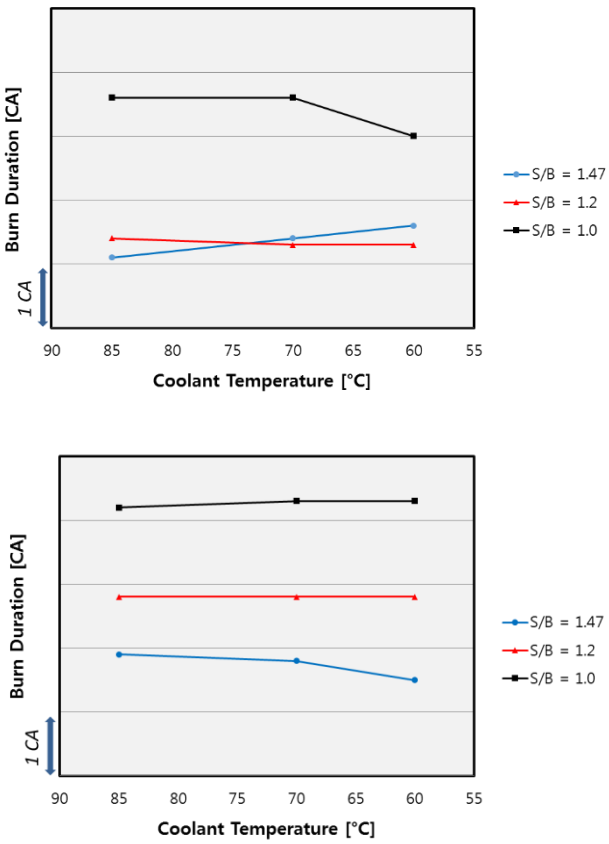

Figure 17. Comparison of burn duration at expanded load limit (a) 1500 rpm, (b) 2000 rpm

Piston oil-cooling gallery

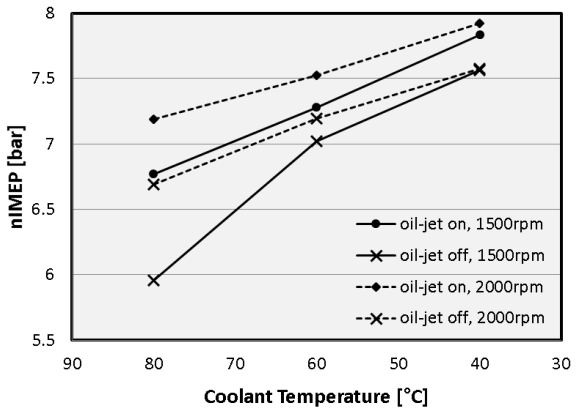

Figure 18. Knock mitigation effect of piston oil-cooling gallery.

For the oil-cooing gallery of the piston in this study, the oil was injected from the engine block to the intake side and flows through the gallery. The engine A (PFI) was used for the implementation. The result is shown in Fig. 17. Both of the coolant temperatures were decreased from 80℃ to 40℃. In this implementation, the compression ratio was 12.5. Under the same level of knock incidence of 10%, the load limit could be expanded from 5.96 bar to 6.59 bar (10%) at 1500 rpm and 6.69 to 7.19 bar (7.5%) at 2000 rpm, which is a large expansion.

Summary/Conclusions

1. In this study, knock detection methods using in-cylinder pressure sensors were reviewed, specifically in terms of the knock intensity and knock onset determination for real engine tests. A steady-state experiment method using knock incidence was newly proposed.

(1) A 4~28 kHz 5th-order Butterworth band-pass filter was used. MAPO TVE 0.5 bar method can provide precise detection of weak knock. Knock incidence calculated from this detection method can be used to measure knock tendency with high reliability.

(2) Knock onset determination using a 9-point median and 7-point 2nd-order Savizky-Golay smoothing filter can effectively determine knock onset. This can be used during an engine test in real time.

2. Measurements of cylinder wall temperatures was conducted to verify the thermal effect of segregated cooling of the cylinder head and liner.

(1) Independent controlling of the wall temperatures was well achieved. Liner coolant temperature was found to have a large effect on the piston surface while the head coolant temperature doesn't.

(2) By oil jet injection into piston oil-cooling gallery, significant drop of piston surface temperature was achieved which showed the larger effect than the decrease of liner coolant temperature.

3. The knock mitigation effect was quantified with two methods: ignition timing advance and load limit expansion. Through these two methods, the effect of the head and the liner could be separated. As a result, it shows that the temperature of the coolant head is more influential than that of the liner. However, temperature measurements also show that liner cooling also has potential for knock mitigation.

(1) 0.2, 0.12, 0.11 CA /℃ of ignition timing advance per decrease of unit coolant temperature was achieved under 1500 rpm in simultaneous cooling, head coolant cooling and liner coolant cooing, respectively. The effect was larger in 2000 rpm. (0.26 CA, 0.21 CA, 0.18 CA /℃ in 2000 rpm) This resulted in 2.89% and 3.45% decrease of ISFC.

(2) 10.3% and 6.8% of the load limit expansion was achieved 1500 rpm and 2000 rpm, respectively, in a simultaneous cooling case. A 7.1% and 4.8% increase for head coolant cooling and a 4.8% and 2.5% increase for liner coolant cooling were achieved at the speed conditions.

4. Knock mitigation effects were also investigated in different types of engines through the load limit expansion tests.

(1) In the GDI engine test, the head coolant temperature showed the larger effect than the liner coolant temperature as well. However, further mitigation than PFI engine was shown when the simultaneous cooling was adapted.

(2) For higher S/B ratios, load limit was expanded under the same condition of coolant temperatures mainly due to enhanced combustion period. The effect of coolant temperature decrease was similar in all S/B ratios.

(3) Piston cooling through the oil-cooling gallery showed a significant effect. Approximate 25℃ decrease of mean piston surface temperature was achieved, resulted in 10% and 7.5% of load limit expansion at 1500 and 2000 rpm, respectively.

References

1. Heywood, J.B., Internal Combustion Engine Fundamentals, 1988: McGraw-Hill
2. Liu, H., Wang, Z., Long, Y., Qi, Y. et al., "Role of Wall Effect on Hot-Spot Induced Deflagration to Detonation in Iso-Octane/Air Mixture Under High Temperature and Pressure," SAE Technical Paper 2016-01-0552, 2016, doi:10.4271/2016-01-0552.
3. McKenzie, J. and Cheng, W., "The Anatomy of Knock," SAE Technical Paper 2016-01-0704, 2016, doi:10.4271/2016-01-0704.
4. Zeldovich, YA., "Regime Classification of an Exothermic Reaction with Nonuniform Initial Conditions," Combustion and Flame, 39(2), 211-214, 1980, doi:10.1016/0010-2180(80)90017-6
5. König, G., Maly, R., Bradley, D., Lau, A. et al., "Role of Exothermic Centres on Knock Initiation and Knock Damage," SAE Technical Paper 902136, 1990, doi:10.4271/902136.
6. Nate, R. and Yates, A., "Knock Damage Mechanisms in Spark-Ignition Engines," SAE Technical Paper 942064, 1994, doi:10.4271/942064
7. Fitton, J. and Nates, R., "Knock Erosion in Spark-ignition Engines," SAE Technical Paper 962102, 1996, doi:10.4271/962102
8. Wang, Z., Liu, H., and Reitz, R., "Knocking Combustion in Spark-ignition Engines," Progress in Energy and Combustion Science, 61, 78-112, 2017, doi:10.1016/j.pecs.2017.03.004
9. Asif, M., Giles, K., Lewis, A., Akehurst, S., et al., "Influence of Coolant Temperature and Flow Rate, and Air Flow on Knock Performance of a Downsized, Highly Boosted, Direct-Injection Spark Ignition Engine," SAE Technical Paper 2017-01-0664, 2017, doi:10.4271/2017-01-0664.
10. Hwang, K., Hwang, I., Lee, H., Park, H. et al., "Development of New High-Efficiency Kappa 1.6L GDI Engine," SAE Technical Paper 2016-01-0667, 2016, doi:10.4271/2016-01-0667.
11. Niizato, T., Yasui, Y., Urata, Y., Wada, Y. et al., "Honda's New Turbo-GDI Engine Series for Global Application," 37th International Vienna Motor Symposium, 2016
12. Burrows, J., Mixell, K., Reinicke, P., Riess, M. et al, "Corona Ignition – Assessment of Physical Effects by Pressure Chamber, Rapid Compression Machine, and Single Cylinder Engine Testing," 2nd International Conference on Ignition Systems for Gasoline Engines, 2014
13. Schenk, M., Wolf, T., Schroter, M., Zellinger,F. et al., "Corona-Ignition vs. Spark Ignition: A Fundamental Comparison for varying thermodynamic conditions of modern turbocharged Gasoline Engines," SIA Powertrain Conference, 2015
14. Ikeya, K., Takazawa, M., Yamada, T., Park, S. et al., "Thermal Efficiency Enhancement of a Gasoline Engine," SAE Int. J. Engines 8(4):2015, doi:10.4271/2015-01-1263.
15. Yoshihara, Y., Nakata, K., Takahashi, D., Omura, T. et al., "Development of High Tumble Intake-Port for High Thermal Efficiency Engines," SAE Technical Paper 2016-01-0692, 2016, doi:10.4271/2016-01-0692.
16. Takahashi, D., Nakata, K., Yoshihara, Y., and Omura, T., "Combustion Development to Realize High Thermal Efficiency Engines," SAE Int. J. Engines 9(3):2016, doi:10.4271/2016-01-0693.
17. Omura, T., Nakata, K., Yoshihara, Y., and Takahashi, D., "Research on the Measures for Improving Cycle-to-Cycle Variations under High Tumble Combustion," SAE Technical Paper 2016-01-0694, 2016, doi:10.4271/2016-01-0694
18. Nakata, K. and Shimizu, R., "Toyota's New Combustion Technology for High Engine Thermal Efficiency and High Engine Output Performance," 37th International Vienna Motor Symposium, 2016
19. Adachi, S. and Hagihara, H., "The renewed 4-Cyilnder Engine Series for Toyota Hybrid System," 33th International Vienna Motor Symposium, 2012
20. Takahashi, D., Nakata, K., Yoshihara, Y., Ohta, Y. et al., "Combustion technology to achieve engine thermal efficiency of 40% for HVs engine," SIA Powertrain Conference, 2015
21. Matsuo, S., Ikeda, E., Ito, Y., and Nishiura, H., "The New Toyota Inline 4 Cylinder 1.8L ESTEC 2ZR-FXE Gasoline Engine for Hybrid Car," SAE Technical Paper 2016-01-0684, 2016, doi:10.4271/2016-01-0684.
22. Kobayashi, H., Yoshimura, K., and Hirayama, T., "A study on dual circuit cooling for higher compression ratio," SAE Technical Paper 841294, 1984, https://doi.org/10.4271/841294.
23. Finlay, I., Gallacher, G., Biddulph, T., and Marshall, R., "The Application of Precision Cooling to the Cylinder-Head of a Small, Automotive, Petrol Engine," SAE Technical Paper 880263, 1988, https://doi.org/10.4271/880263.
24. Iwashita, Y., Kanda, M., Hartagiri, H., and Yokoi, Y., "Improvement of Coolant Flow for Reducing Knock," I. Mech. E. Autotech Conference, 1989.
25. Kubozuka, T., Ogawa, N., Hirano, Y., and Hayashi, Y., "The Development of Engine Evaporative Cooling System," SAE Technical Paper 870033, 1987, https://doi.org/10.4271/870033.
26. Russ, S., "A Review of the Effect of Engine Operating Conditions on Borderline Knock," SAE Technical Paper 960497, 1996, https://doi.org/10.4271/960497.
27. Fukuda, Y., Tawa, H., and Makise, A., "Increase of Knock Limit in Outboard Motor Through Employment of Dual Control Direct Cooling System," Honda Technical Paper, Vol. 16, No. 1, 2004.
28. Takahashi, D., Nakata, K., and Yoshihara, Y., "Engine Thermal Control for Improving the Engine Thermal Efficiency and Anti-Knocking Quality," SAE Technical Paper 2012-01-0377, 2012, doi:10.4271/2012-01-0377
29. Imaoka, Y., Shouji, K., Inoue, T., and Noda, T., "A Study of Combustion Technology for a High Compression Ratio Engine: The Influence of Combustion Chamber Wall Temperature on Knocking," SAE Int. J. Engines 9(2):2016, doi:10.4271/2016-01-0703.
30. Cho, S., Song, C., Min, K., Kim, M., et al., "The Effect of Thermal Boundary Conditions on Knock Characteristics in a Single Cylinder Spark Ignited Engine," SIA Powertrain Conference, 2017
31. Kalghatgi, G., Algunaibet, I., and Morganti, K., "On Knock Intensity and Superknock in SI Engines," SAE Int. J. Engines 10(3):2017, doi:10.4271/2017-01-0689.
32. Brunt, M., Pond, C., and Biundo, J., "Gasoline Engine Knock Analysis using Cylinder Pressure Data," SAE Technical Paper 980896, 1998, doi:10.4271/980896.
33. Bertola, A., Stadler, J., Walter, T., Wolfer, P. et al., "Pressure Indication during Knocking Conditions," KISTLER Special Print No. 920-349e-11.06.

34. Zhen, X., Wang, Y., Xu, S., Zhu, Y. et al., "The engine knock analysis – An overview," Applied Energy, 92, 628-636, 2012, doi:10.1016/j.apenergy.2011.11.079.
35. Kim, K., "Study of Engine Knock Using a Monte Carlo Method," Ph.D. Dissertation, University of Wisconsin-Madison, 2015.
36. Draper, C., "The Physical Effects of Detonation in a Closed Cylindrical Chamber," NASA Report No. 493, 1934.
37. Millo, F. and Ferraro, C., "Knock in S.I. Engines: A Comparison between Different Techniques for Detection and Control," SAE Technical Paper 982477, doi:10.4271/982477.
38. Eng, J., "Characterization of Pressure Waves in HCCI Combustion," SAE Technical Paper 2002-01-2859, doi: 10.4271/2002-01-2859.
39. Gaeta, A., Giglio, V., Police, G. and Rispoli, N., "Modeling of in-Cylinder pressure oscillation under knocking conditions: A general approach based on the damped wave equation," Fuel, 104, 230-243, 2013, doi:10.1016/j.fuel.2012.07.066.
40. Zucrow, M., Hoffman, J., Gas Dynamics, Volume 2 – Multidimensional Flow, 1977, John Wiley and Sons.
41. Shahlari, A. and Ghandhi, J., "Pressure-Based Knock Measurement Issues," SAE Technical Paper 2017-01-0668, 2017, doi:10.4271/2017-01-0668.
42. Ando, H., Takemura, J., and Koujina, E., "A Knock Anticipating Strategy Basing on the Real-Time Combustion Mode Analysis," SAE Technical Paper 890882, 1989, doi:10.4271/890882.
43. Sjöberg, M., Vuilleumier, D., Yokoo, N. and Nakata, K., "Effects of Gasoline Composition and Octane Sensitivity on the Response of DISI Engine Knock to Variations of Fuel – Air Equivalence Ratio," 9th International Conference on Modeling and Diagnostics for Advanced Engine Systems (COMODIA), 2017.
44. Kirsten, M., Pirker, G., Redtenbacher, C., Wimmer, A. et al., "Advanced Knock Detection for Diesel/Natural Gas Engine Operation," SAE Int. J. Engines 9(3):2016, doi:10.4271/2016-01-0785.
45. Shahlari, A. and Ghandhi, J., "A Comparison of Engine Knock Metrics," SAE Technical Paper 2012-32-0007, 2012, doi:10.4271/2012-32-0007.
46. Worret, R., Bernhardt, S., Schwarz, F., and Spicher, U., "Application of Different Cylinder Pressure Based Knock Detection Methods in Spark Ignition Engines," SAE Technical Paper 2002-01-1668, 2002, doi: 10.4271/2002-01-1668.
47. Lee, J., Hwang, S., Lim, J., Jeon, D. et al., "A New Knock-Detection Method using Cylinder Pressure, Block Vibration and Sound Pressure Signals from a SI Engine," SAE Technical Paper 981436, 1998, doi:10.4271/981436.
48. Borg, J. and Alkidas, A., "Cylinder-pressure-based Methods for Sensing Spark-ignition Engine Knock," International journal of vehicle design, 45.1-2, 222-241, 2007, doi:10.1504/IJVD.2007.013678.
49. Amann, M. and Alger, T., "Lubricant Reactivity Effects on Gasoline Spark Ignition Engine Knock," SAE Int. J. Fuels Lubr. 5(2):760-771, 2012, doi:10.4271/2012-01-1140.
50. Brecq, G., Bellettre, J. and Tazerout, M., "A new indicator for knock detection in gas SI engines," International Journal of Thermal Sciences, 42(5), 523-532, 2003, doi:10.1016/S1290-0729(02)00052-2.
51. Hudson, C., Gao, X. and Stone, R., "Knock Measurement for Fuel Evaluation in Spark Ignition Engines," Fuel, 80, 395-407, 2001, doi:10.1016/S0016-2361(00)00080-6.
52. Bradley, D., Kalghatgi, G., "Influence of autoignition delay time characteristics of different fuels on pressure waves and knock in reciprocating engines," Combustion and Flame, 156, 2307-2318, 2009, doi:10.1016/j.combustflame.2009.08.003
53. Mutzke, J., Scott, B., Stone, R., and Williams, J., "The Effect of Combustion Knock on the Instantaneous Heat Flux in Spark Ignition Engines," SAE Technical Paper 2016-01-0700, 2016, doi:10.4271/2016-01-0700.
54. Kalghatgi, G., Morganti, K., and Algunaibet, I., "Some Insights on the Stochastic Nature of Knock and the Evolution of Hot Spots in the End-Gas During the Engine Cycle from experimental Measurements of Knock Onset and Knock Intensity," SAE Technical Paper 2017-01-2233, 2017, doi:10.4271/2017-01-2233.
55. Brunt, M. and Lucas, G., "The Effect of Crank Angle Resolution on Cylinder Pressure Analysis," SAE Technical Paper 910041, 1991, doi:10.4271/910041.
56. Lancaster, D., Krieger, R., and Lienesch, J., "Measurement and Analysis of Engine Pressure Data," SAE Technical Paper 750026, 1975, doi:10.4271/750026.
57. Skoog, D., Leary, J., "Principles of Instrumental Analysis," 4th Edition, 1992, Saunders College Publishing.

Contact Information

Seokwon Cho
seokwon@snu.ac.kr

Kyoungdoug Min
kdmin@snu.ac.kr

Acknowledgments

This work was supported by the Advanced Automotive Research Center (AARC) and Institute of Advanced Machinery and Design (IAMD) of Seoul National University. The engines for this study were donated by the Hyundai Motor Group. The authors would like to express our sincere gratitude to them.

Definitions/Abbreviations

aBDC	after bottom dead center
aTDC	after top dead center
bBDC	before bottom dead center
bTDC	before top dead center
CA	crank angle
CR	compression ratio
CFD	computational fluid dynamics
CO	carbon oxide
CVVT	continuous variable valve timing
DISI	direct injection spark ignition

DKI	dimensionless knock indicator
ECU	engine control unit
EGR	exhaust gas recirculation
EVC	exhaust valve closing
EVO	exhaust valve opening
GDI	gasoline direct injection
H/C	hydrogen/carbon
IMEP	indicated mean effective pressure
IMPO	integral of modulus pressure oscillation
ISFC	indicated specific fuel consumption
ISPO	integral of squared pressure oscillation
IVC	intake valve closing
IVO	intake valve opening
KI	knock intensity
KLSA	knock limit spark advance
LHV	low heating value
LIVC	late intake valve closing
LKI	logarithmic knock intensity
MAPO	maximum amplitude of pressure oscillation
MBT	maximum brake torque
MFB50	mass fraction burned 50%
PCB	printed circuit board
PDF	power density function
PFI	port fuel injection
PM	particulate emission
S/B	stroke-to-bore
SER	signal energy ratio
SI	spark ignited
SOC	start of combustion
TDC	top dead center
THC	total hydrocarbon
TVE	threshold value exceed
WOT	wide open throttle